Available online at www.sciencedirect.com
SCIENCE DIRECT®
Journal of Crystal Growth 271 (2004) 474–480
JOURNAL OF CRYSTAL GROWTH
www.elsevier.com/locate/jcrysgro

Reversing radial segregation and suppressing morphological instability during Bridgman crystal growth by angular vibration

W.C. Yu[a], Z.B. Chen[a], W.T. Hsu[b], B. Roux[c], T.P. Lyubimova[d], C.W. Lan[b,*]

[a]*Department of Molecular Science and Engineering, National Taipei University of Technology, Taiwan*
[b]*Department of Chemical Engineering, National Taiwan University, Taipei, Taiwan, 10617, ROC*
[c]*Laboratoire Modélisation et simulation numérique en mécanique, L3M/FRE 2405 MSNM: CNRS-Universités d'Aix-Marseille, France*
[d]*Institute of Continuous Media Mechanics UB RAS, Perm, Russia*

Received 12 June 2004; accepted 22 July 2004
Communicated by D.T.J. Hurle
Available online 25 September 2004

Abstract

During vertical Bridgman crystal growth, local solute accumulation along the freezing interface due to buoyancy often causes radial non-uniformity and pit formation, which accelerate morphological instability. A novel approach by using angular vibration has been proposed. Through the visualization of the freezing interface during directional solidification of succinonitrile containing acetone, it was shown that angular vibration about the growth axis was effective in reversing radial segregation and thus enhancing morphological stability. Simulation was conducted and good agreement was found.

PACS: 44.25.+f; 47.27.Te; 81.10.Fq; 02.60.c6; 02.70Fj

Keywords: A1. Computer simulation; A1. Convection; A1. Directional solidification; A1. Heat transfer; A1. Interfaces; A1. Mass transfer; A1. Morphological stability; A2. Bridgman technique; A2. Gradient freeze technique; A2. Growth from melt; B1. Organic compounds

1. Introduction

The control of segregation and morphological instability is important in vertical Bridgman crystal growth. Due to buoyancy convection, local solute accumulation along the freezing interface often causes radial non-uniformity and pit formation, which accelerate morphological instability through constitutional supercooling [1–4]. To avoid the severe radial segregation and pit formation, the control of convection patterns and solute

*Corresponding author. Tel./fax: +886-2-2363-3917.
E-mail address: cwlan@ntu.edu.tw (C.W. Lan).

0022-0248/$ - see front matter © 2004 Elsevier B.V. All rights reserved.
doi:10.1016/j.jcrysgro.2004.07.080

transport near the growth front is necessary. The use of external forces is an effective way for convection control. For example, magnetic fields have been widely adopted for electrically conducting materials [5]. The use of a centrifuge [6,7], i.e., the so-called centrifugal or high-gravity processing, is also popular. In a recent study by Lan and coworkers [8,9], rotation about the growth axis was found more effective than the previous free-swing configurations, where the resultant gravity is parallel to the growth axis. In addition to minimizing the flow intensity, the flow direction near the solidification front could be reversed at high speed rotation. As a result, morphological stability could be greatly enhanced [9]. Nevertheless, a relatively high rotation speed (in the order of 100 rpm) is often necessary for applications.

Another way to use rotation for flow control is the accelerated crucible rotation technique (ACRT) [10]. It generates Ekman flow near the solidification front and Taylor Görtler cells near the ampoule wall during crucible acceleration and deceleration, which are also effective in solute mixing [11,12]. However, periodic growth rate and growth striations are the problems for crystal quality [11,12]. Recently, the coupled vibrational stirring (CVS) was also proposed [13] using asymmetric rotational motion, which generates flushing waves at the upper melt surface and thus enhances solute mixing. Unfortunately, CVS generates vigorous convection that is not favored for axial segregation control. To reduce axial segregation, global solute mixing needs to be minimized [6,7]. Moreover, unstable growth rate was also observed in the CVS-controlled oxide growth [13].

In this report, we propose a novel technique by using angular vibration about the ampoule axis to control the flow and segregation in a vertical Bridgman crystal growth. As will be shown, this technique is simple and effective. In addition to the inversion of radial segregation, the angular vibration has only a small effect on global solute mixing, so that it is not harmful to axial segregation if the growth distance is long enough. Due to better solute uniformity, morphological stability is further enhanced.

2. Experiments and numerical simulations

Succinonitrile (SCN) containing 0.007 wt% acetone was directionally solidified in a transparent vertical Bridgman system, as shown in Fig. 1. Before experiments, SCN (Furuka Inc., about 99% purity) was purified first by vacuum distillation at 50 mTorr for ten times. The sample purity was checked by the melting point using a thermistor showing the sample purity is higher

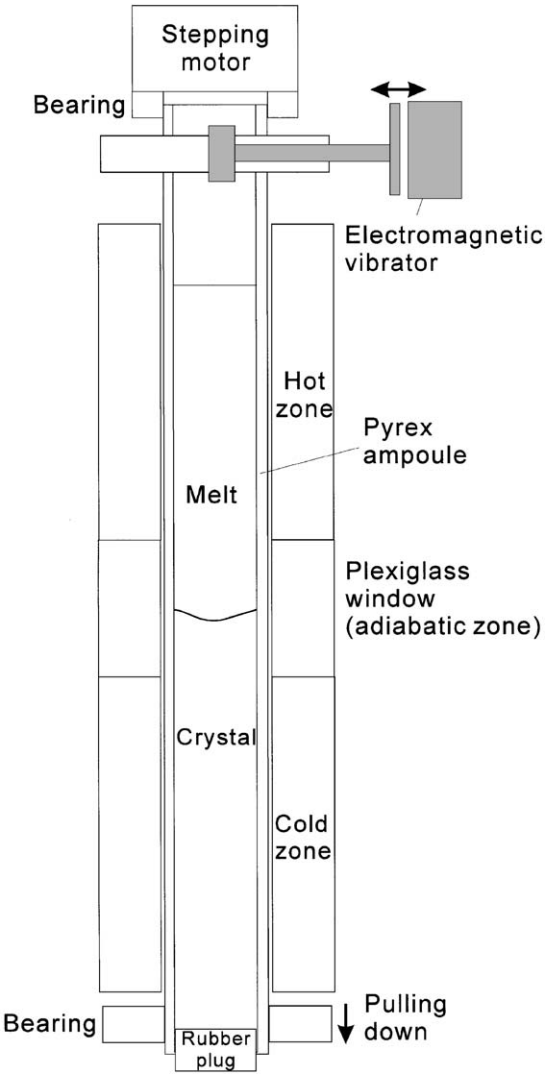

Fig. 1. Sketch of the experimental setup for vertical Bridgman crystal growth with angular vibration.

than 99.999% [14]. The distilled sample, collected in a 17 mm diameter Pyrex ampoule (2.5 mm in thickness), was further purified by four-zone refining for more than 60 passes. The purified sample was then examined by directional solidification. No morphological breakdown was observed up to 15 μm/s of the solidification speed for a thermal gradient of 8–10 K/cm. To perform crystal growth experiments, about 0.007 wt% of acetone was injected into the sample through a 5 μl micro-syringe inserted into the bottom of the sample. The total sample length was 20 cm.

The Bridgman furnace consisted of two heating zones made of copper blocks each with a nichrome wire inside as a heating element. In between, a transparent insulation zone made of Plexiglas was used. The hot- and cold-zone temperatures were controlled independently by two PID controllers and the temperatures were set at 80 °C (top) and 40 °C (bottom), respectively. The thermal gradient at the interface was measured by an immersed thermocouple traveling with the sample. By taking an average of the gradients at the interface from solidification and melting curves, we estimated the thermal gradient to be about 8–10 K/cm. To translate the ampoule accurately, a microstepping motor was used to drive a screw slide; the translation rate was controlled at 2.5 μm/s in this study. During crystal growth, a video camera recorded the evolution of the interface morphology with a back lighting to enhance the contrast of the image. Also, to allow smooth vibration in the rotational (angular) direction, the ampoule was tightly fitted into a pair of bearings (top and bottom) that were both mounted on the translating system. Then, to generate angular vibration, an electromagnetic vibrator, which was also mounted on the translating system, was used. Its shaft was connected to a mounting disk and the vibration amplitude was controlled by a variac, while the frequency was fixed at 60 Hz. The vibration amplitude was estimated by measuring the width of a vertical thin mark from the video image during vibration.

For better understanding the observed phenomena, an axisymmetric numerical model accounting for melt convection, heat and mass transfer, and the moving interface [4,15] was used to simulate the crystal growth process. However, direct numerical simulation using the no-slip velocity boundary on the interface, i.e.,

$$V_\theta = \alpha\omega r \sin \omega t, \tag{1}$$

is too time consuming for growth simulation because the oscillation period is only 1/60 s. In Eq. (1), V_θ is the angular velocity, α the normalized amplitude (a fraction of 2π), ω the angular frequency, r the radial distance, and t the time; $\alpha\omega$ is equivalent to the rotation speed. Instead of using this boundary condition, we have derived an effective slip condition based on the treatment in the Schlichting flow [16], where an average tangential (radial) streaming velocity V_t at the growth front can be written as

$$V_t = \frac{\pi}{2}\alpha^2 f r \sin \phi, \tag{2}$$

where f is the frequency of vibration and ϕ the angle between the tangent of the front and growth axis; $f = \omega/2\pi$. Eq. (2) is valid when the frequency is high enough so that the Schlichting layer thickness, i.e., $\sim \sqrt{v/\pi f}$, is small as compared with the domain for convection; v is the kinematic viscosity of the melt. Direct numerical simulation using Eq. (1) was also carried out for the comparison with the one using the effective boundary condition (Eq. (2)), and good agreement was found. Also, the heating profile was described by a hyperbolic tangent function fitting to the measured one having the thermal gradient at the interface near 10 K/cm. The upper melt surface was set to be stress-free, while the no-slip boundary condition was adopted for other solid boundaries. With these boundary conditions, the problem was solved by an efficient finite volume method. Detailed discussion of the numerical model and the comparison with the experiments can be found elsewhere [9,15].

3. Results and discussion

Fig. 2 shows the interface evolution without angular vibration. As shown, before solidification was started, the interface was flat because the thermal conductivities of the melt and the crystal

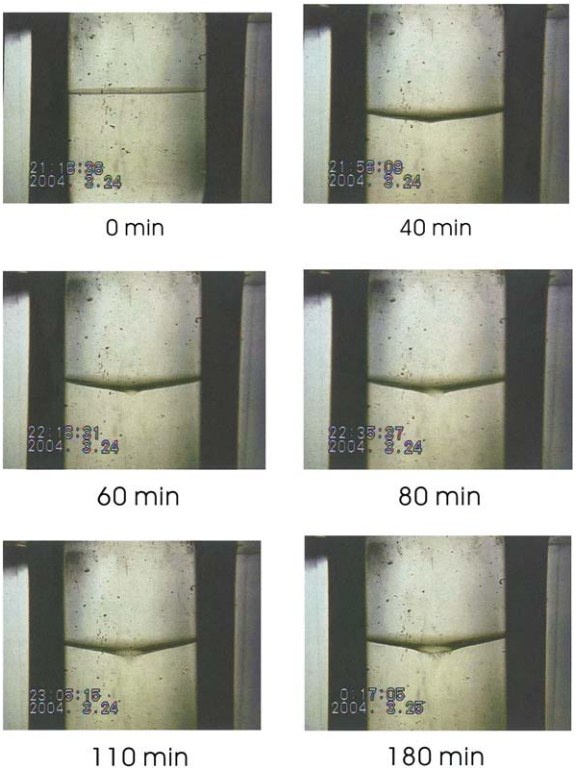

Fig. 2. Interface evolution for SCN containing 0.007 wt% acetone without angular vibration at an ampoule pulling speed of 2.5 μm/s.

are very close to each other [3]. As the ampoule translated at 2.5 μm/s, the solidification began and the interface became concave due to the release of heat of fusion, as shown by the photograph at 40 min. Meanwhile, a clear depression or pit formed at the interface center. This pit formation is due to acetone accumulation, which lowers the solidification temperature. A similar observation was reported by Schaefer and Coriell [3] for SCN/EtOH and by Singh et al. [17] for $PbBr_2$/AgBr. As the solidification proceeded further, more solute was accumulated in front of the interface, because the acetone has a lower solubility in the solid than that in the melt (the segregation coefficient is 0.1) [3]. Finally, as shown by the photograph at 80 min, the freezing interface at the tip of the pit started to breakdown. A clear dendritic structure was observed at the bottom of the pit as the solidification continued further, as shown by the photographs at 110 and 180 min in Fig. 2.

With angular vibration, a similar experiment was performed; the normalized vibration amplitude α is about 0.0157. The use of this condition was estimated from Eq. (2) that the maximum tangential velocity (about 0.02 cm/s) is large enough to reverse the melt velocity due to the buoyancy force. Interestingly, as the vibration was applied, a concave and wavy interface appeared, as shown in Fig. 3 (0 min). The wavy pattern became clearer right after the solidification started, but decayed slowly as that shown in Fig. 2 (20 min). After 30 min, the wavy pattern disappeared and the solidification front became smooth. As the solidification proceeded further at 40 min, the interface became more concave, and the wavy patterns remained invisible. Such an interface remained stable for more than 3 h of observation

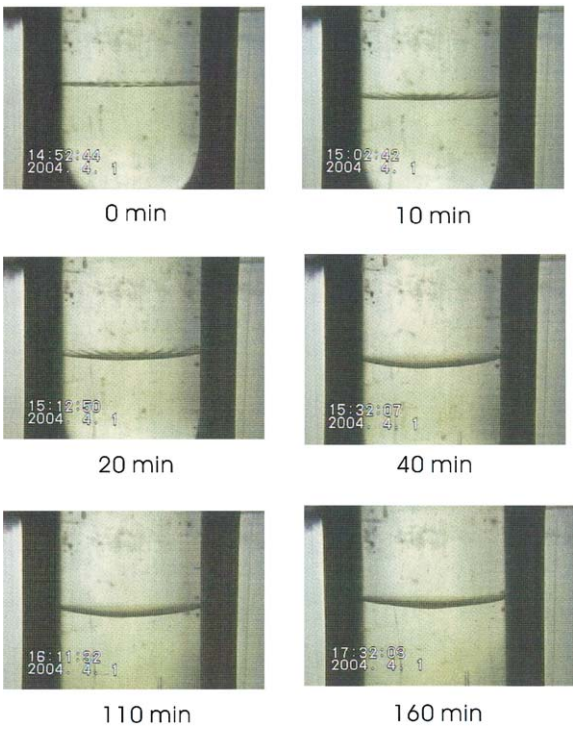

Fig. 3. Interface evolution for SCN containing 0.007 wt% acetone with angular vibration at an ampoule pulling speed of 2.5 μm/s; vibration amplitude is about 0.0157 and frequency 60 Hz.

time. Clearly, pit formation was prevented and the local solute accumulation did not occur at the interface center. As a result, the interface morphology was stable.

A set of simulations was also carried out to explain the above observations. The simulated results corresponding to the cases in Figs. 2 and 3 are shown in Figs. 4a and b, respectively. In each plot, the left-hand side shows the flow patterns (stream function Ψ) and the right-hand side the normalized acetone concentration (C/C_0); $C_0 =$ 0.007 wt% the initial concentration. As shown in Fig. 4a, without ampoule translation, the convection near the interface is weak, while the flow prevails near the upper edge of the adiabatic zone. The upper flow cell is in the clockwise direction (negative Ψ), while the lower one counterclockwise (positive Ψ). As the ampoule translates, the interface becomes concave, and buoyancy convection near the interface is induced. Meanwhile, the solute is rejected from the solidification front and is pushed toward the interface center leading to a pit formation at the center. The pit becomes sharper as the solidification proceeds further until numerical breakdown is encountered due to the wriggled interface (the last plot). On the other hand, when the vibration is considered, a strong Schlichting flow appears, as shown by the lower flow cell (clockwise in the direction) in Fig. 4b. Because the mean streaming velocity, whose intensity is from Eq. (2), is considered at the interface, a flow cell is induced and its direction is opposite to the thermal convection one. As a result, the interface became slightly concave even without ampoule translation. Such a flow continues to prevail near the interface even with ampoule translation. As shown in Fig. 4b during solidification, the solute rejected is carried away from the center to the peripheral of the interface. Because the solute accumulation at the center is prevented, no pit is formed there. Due to the release of heat of fusion, the interface concavity

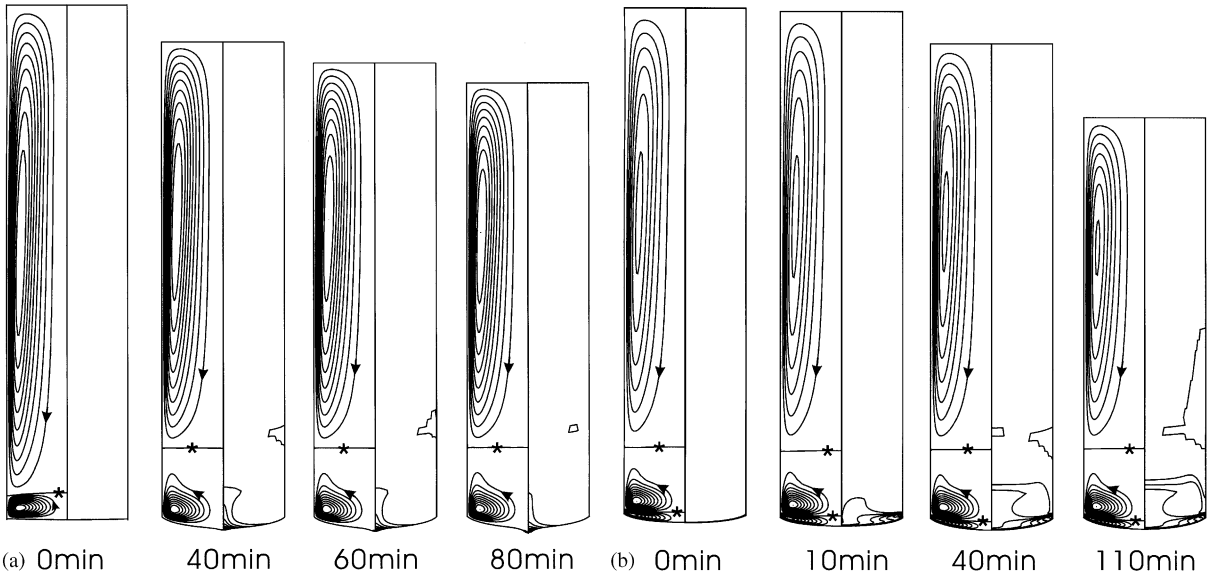

Fig. 4. Simulation results for SCN growth: (a) without vibration; (b) with vibration; on the left hand side of each plot is the contours of stream function (Ψ) (* indicates the zero streamline) and on the right-hand side the normalized acetone concentration (C/C_0); C_0 is the initial acetone concentration. In (a), $\Psi_{\min}(\Psi_{\max}) = -1.799 \times 10^{-4}$ (2.996×10^{-5}) g/s, -1.327×10^{-4} (4.482×10^{-4}) g/s, -1.326×10^{-4} (4.528×10^{-4}) g/s, and -1.320×10^{-4} (4.509×10^{-4}) g/s, while the maximum C/C_0 is 1, 14.87, 22.73, and 35.9241, from the left to the right for each plot, respectively. In (b), $\Psi_{\min}(\Psi_{\max}) = -2.803 \times 10^{-4}$ (7.905×10^{-5}) g/s, -2.108×10^{-4} (3.212×10^{-4}) g/s, -1.823×10^{-4} (4.293×10^{-4}) g/s, and -1.816×10^{-4} (4.374×10^{-4}) g/s, while the maximum C/C_0 is 1, 1.825, 3.799, and 6.206, from the left to the right, respectively.

also increases slowly with time, and this is consistent with the observation.

If one examines carefully the acetone concentration at the growth interface in Fig. 4, it is clear that the acetone accumulation during pit formation is much larger than that without a pit under angular vibration. Further comparison is illustrated in Fig. 5 on the radial acetone concentration at different growth periods from Fig. 4. As shown, without vibration the acetone accumulates quickly as the solidification proceeds at the interface center, while no local acetone accumulation is observed for the cases with vibration. The radial segregation is indeed reversed by the vibration, and the acetone concentration increases slowly from the centerline to the ampoule wall. Furthermore, as shown in Fig. 5 the averaged acetone concentration at the interface is not much affected by vibration indicating that the global acetone mixing is not enhanced. This can also be seen from the concentration fields in Fig. 4b. The vibration has only a small effect on the bulk concentration away from the interface. More importantly, because the frequency is high, the fluctuations of the solute concentration and solidification speed marked on the solidifying crystal may not be detrimental to its quality. For most materials at high temperature, solid state diffusion should be fast enough to smooth out these fluctuations.

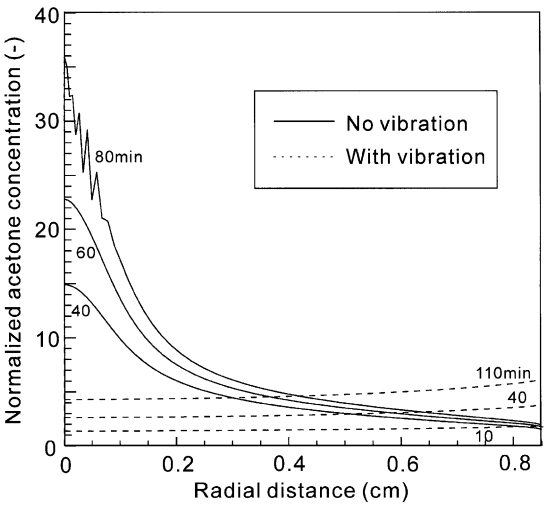

Fig. 5. Comparison of radial acetone concentration (C/C_0) at the interface for different solidification times from Fig. 4; $C_0 = 0.007$ wt%.

4. Conclusion

In this report, angular (rotational) vibration for flow and segregation control during vertical Bridgman crystal growth has been proposed and verified by using a transparent system and numerical simulation. As compared with the traditional active control approaches, angular vibration is simpler, but more effective. It is also easy to implement angular vibration in an existing system. The radial segregation can be controlled easily by the amplitude or frequency. Furthermore, because the global solute mixing is not enhanced, the present approach does not increase the axial segregation. Meanwhile, due to the high frequency, solidification speed is stable, and the crystal quality could be preserved.

Acknowledgements

This work was supported by the National Science Council of the Republic of China. CWL also acknowledges the support from Marseillie University for his sabbatical leave in the February of 2004.

References

[1] W.A. Tiller, K.A. Jackson, J.W. Rutter, B. Chalmers, Acta Metall. 1 (1953) 428.
[2] W.W. Mullins, R.F. Sekerka, J. Appl. Phys. 35 (1964) 444.
[3] R.J. Schaefer, S.R. Coriell, Metall. Trans. 15A (1984) 2109.
[4] C.W. Lan, C.Y. Tu, J. Crystal Growth 220 (2000) 619.
[5] A.F. Witt, H.C. Gatos, M.C. Lavine, C.J. Herman, J. Electrochem. Soc. 122 (1975) 296.
[6] H. Rodot, L.L. Regel, G.V. Sarafanov, H. Hamidi, I.V. Videskii, A.M. Turtchaninov, J. Crystal Growth 79 (1986) 77.
[7] J. Friedrich, J. Baumgartl, H.-J. Leister, G. Müller, J. Crystal Growth 167 (1996) 45.
[8] C.W. Lan, C.Y. Tu, J. Crystal Growth 226 (2001) 406.
[9] C.W. Lan, Y.W. Yang, H.Z. Chen, I.F. Lee, Metall. Mater. Trans. A 33 (2002) 3011.
[10] H.J. Scheel, J. Crystal Growth 13 (1971) 304.

[11] C.W. Lan, J.H. Chian, J. Crystal Growth 203 (1999) 286.
[12] A. Yeckel, J.J. Derby, J. Crystal Growth 209 (2000) 734.
[13] K.T. Zawilski, M. Claudia, C. Custodio, R.C. DeMattei, R.S. Feigelson, J. Crystal Growth 258 (2003) 211.
[14] Y.W. Lee, R. Ananth, W.N. Gill, Chem. Eng. Comm. 152 (1996) 41.
[15] C.W. Lan, M.C. Liang, J. Crystal Growth 186 (1998) 187.
[16] G.Z. Gershuni, D.V. Lyubimov, Thermal Vibration Convection, Wiley, New York, 1998.
[17] N.B. Singh, S.S. Mani, J.D. Adam, S.R. Coriell, M.E. Glicksman, W.M.B. Duval, G.J. Santoro, R. DeWitt, J. Crystal Growth 166 (1996) 364.